Dripping to jetting transition for cross-flowing liquids

Aude Bertrandias, H. Duval, Joel Casalinho, Marie-Laurence Giorgi

Dripping to jetting transition for cross-flowing liquids

A. Bertrandias,[a] H. Duval,[b] J. Casalinho, and M. L. Giorgi
Laboratoire de Génie des Procédés et Matériaux (LGPM), CentraleSupélec, Université Paris Saclay, Grande voie des vignes, 92295 Châtenay-Malabry, France

Received and accepted dates, other relevant dates

We experimentally study drops formed from a nozzle into an immiscible, cross-flowing phase. Depending on the operating conditions, drops are generated either in dripping or jetting mode. We investigate the impact of the continuous and dispersed phase velocities, dispersed phase viscosity and interfacial tension on the drop generation mode and size. We find that a dripping to jetting transition (DJT) takes place at a critical inner Weber number, function of the outer capillary and Ohnesorge numbers. Two jetting regimes occur depending on the phase velocity ratio. When the continuous phase velocity is significantly greater (resp. lower) than the dispersed phase velocity, jet narrowing (resp. widening) occurs. In jet widening, the critical inner Weber number depends little on the outer capillary number whereas in jet narrowing, it sharply decreases as the outer capillary number increases. We propose a comprehensive model to describe the DJT based on the attached drop equation of motion. The model satisfactorily predicts the DJT and the effect of the outer capillary number on the critical inner Weber number. It also well accounts for the drop diameter in jet narrowing.

I. INTRODUCTION

Membrane emulsification is an industrial process used to generate emulsions by forcing a dispersed phase through an inorganic, porous membrane into a continuous cross-flowing phase.[1] This process is usually operated in dripping (drop by drop) mode. The shear stress exerted by the continuous phase controls drop formation, so drag and the retaining capillary force are the main forces involved. In dripping mode, the drop diameter decreases with increasing shear stress, while remaining greater than the membrane pore size. A first estimate of the drop diameter may be given by a simple torque balance about the pore edge.[2]

More recently, alternative fabrication methods based on microfluidics have appeared, such as flow-focusing and coflowing devices. These devices commonly operate in dripping or jetting (continuous jet) mode.[3–6] In jetting mode, the liquid thread breaks up by Plateau-Rayleigh instabilities. In certain operating conditions, drops much smaller than the nozzle diameter may be produced. The same trend is expected for membrane emulsification operated in jetting mode. Thus, it is of high interest to study the dripping to jetting transition (DJT) in this process.

A DJT can occur if the liquid thread exiting the nozzle grows to a length comparable to its radius and if the pinch-off time is larger than the thread growth time.[7] The simplest case is the dripping faucet, where a dispersed phase flows from a nozzle into a stagnant, immiscible outer phase. Smith and Moss[8] studied mercury jets into gases and found that above a critical velocity (named the jetting velocity), the liquid exits the nozzle as a jet. They proposed an empirical expression for the jetting velocity, which can be recovered from a simple balance between the jet momentum flux and the retaining capillary force. Scheele and Meister[9] investigated the DJT for fifteen liquid-liquid couples and established the jetting velocity from a force balance, which further includes the excess pressure force. The maximum error between their data and predictions is of 30.2%. Richards *et al.*[10] studied drop formation before and after the DJT by computational fluid dynamics (CFD) and obtained drop sizes that compare well with Scheele and Meister's data.[9] Clanet and Lasheras[11] studied the DJT for water flowing from a stainless steel nozzle into air and found that the DJT occurs at a critical inner Weber number We_{in} function of Bond numbers (Bo, Bo_o). We_{in} compares the inner momentum to the capillary force. It is built with the nozzle inner diameter and mean dispersed phase velocity in the

[a] Electronic mail: aude.bertrandias@centralesupelec.fr
[b] Electronic mail: herve.duval@centralesupelec.fr

nozzle. Bo and $\mathrm{Bo_o}$ compare buoyancy to the retaining capillary force. Bo (resp. $\mathrm{Bo_o}$) is built with the nozzle inner (resp. outer) diameter. When the dispersed phase does not wet the nozzle, only Bo is relevant. Clanet and Lasheras[11] extended Taylor's model[12] for the recession of a free, liquid edge. Their model, adapted to drop recession and growth, predicts the jetting velocities. Their calculations are in good agreement with their own data and Scheele and Meister's data[9] (maximum error of 13.7% and 20%, resp.).

In coflowing liquids, Cramer *et al.*[13] examined the critical continuous phase velocity for the DJT. They found that it decreases for increasing dispersed phase flow rates or viscosity ratios $\zeta = \eta_{dp}/\eta_{cp}$ and for decreasing interfacial tensions. Utada *et al.*[3] proposed a state diagram of the DJT in coflowing liquids in a $\mathrm{Ca_{out}}-\mathrm{We_{in}}$ space. $\mathrm{Ca_{out}}$ compares the viscous force (exerted by the outer fluid) to the capillary force. It is built with the nozzle inner diameter, the outer (continuous) phase viscosity and velocity. Two jetting regimes occur depending on the fluid velocity ratio. If the outer velocity is greater than the inner one, the inner liquid is stretched by the outer fluid and jet narrowing occurs. If the outer velocity is lower than the inner one, the outer fluid slows the inner fluid and jet widening occurs.[3,4] In jet widening, Castro-Hernández *et al.*[4] showed that inertial or viscous forces drove the DJT depending on the inner Reynolds number $\mathrm{Re_{in}}$ (built with the mean dispersed phase velocity and nozzle inner diameter). They proposed a unified scaling to predict drop size in both the widening and narrowing regimes (relative errors of 30%). Chen *et al.*[14] studied both regimes by CFD. They noted that drop detachment in jet widening is due to high pressures in the neck whereas in jet narrowing, it is due to velocity differences between the front and rear ends of the neck (linking the drop to the thread).

Two spatiotemporal instabilities may occur in coflowing liquids: an absolute instability (A), with disturbances advected up- and downstream or a convective instability (C), with advection only downstream.[15,16] Linear stability analysis was performed for confined coflowing liquids. Concentric cylindrical capillaries[17] and rectangular channels[18] were studied at low Reynolds numbers. Analysis was extended to when liquid inertia is not negligible.[19] A/C regions were typically provided as a function of the inner and outer phase flow rates. The A (resp. C) region coincides with the dripping (resp. jetting) region identified experimentally. Stability analysis was also performed for unbounded coflowing liquids: jet widening was reported as absolutely unstable and jet narrowing as convectively unstable. The widening regime was actually assimilated to a dripping regime, with drops formed at the end of the fluid thread.[20]

Compared to coflowing liquids, the DJT in membrane emulsification (*i.e.*, for cross-flowing liquids) was very little investigated: Meyer and Crocker[21] performed experiments whereas Pathak[22] examined the DJT by CFD. For both, membrane emulsification was mimicked by forcing a dispersed phase through a single, circular pore of a plane wall sheared by a continuous phase flow. Meyer and Crocker[21] found that the state diagram of the DJT depends on $\mathrm{We_{in}}$ and $\mathrm{Ca_{out}}$, but also on the inner Ohnesorge number Oh_{dp} (ratio of the viscocapillary to inertial-capillary time scale). Both authors proposed a correlation for the DJT by replacing Bo and $\mathrm{Bo_o}$ by $\mathrm{Ca_{out}}$ in Clanet and Lasheras' DJT criterion[11] and by adjusting coefficients. However, no comprehensive models were developed in this configuration.[21,22]

The aim of this work is to study drop generation in cross-flow. The setup consists in a nozzle, which forms dispersed phase drops into a continuous cross-flowing phase. Both dripping and the DJT are studied for various phase velocities, interfacial tensions and dispersed phase viscosities. Dripping data are used to identify the drag force experienced by a drop attached to the nozzle. Then, a physical model is proposed to predict the jetting velocities and drop diameters at the DJT. This enables to gain insight on drop formation in membrane emulsification and more generally on the DJT for cross-flowing liquids.

II. EXPERIMENTAL

The systems investigated are reported in Table I. For the reference system, the continuous and dispersed phases are distilled water and dodecane, respectively. For systems 1 and 2, a surfactant (Sodium dodecyl sulfate, SDS) is added to the continuous aqueous phase to study the effect of the interfacial tension. We note that the SDS concentration of system 1 (resp. 2) is lower (resp. greater) than the critical micellar concentration (CMC) of SDS in water, *i.e.* 2 $\mathrm{g.L^{-1}}$. For both systems, a good

estimate of the interfacial tension when drops form is given by the value of the dynamic interfacial tension at the intermediate plateau.[23,24] This value is greater than the equilibrium value. For system 2, we consider that micelles have no specific impact on the process examined: surfactant essentially modifies the intermediate plateau value. Last, for systems 3 and 4, paraffin is added to dodecane to study the effect of the dispersed phase viscosity.

We note γ the interfacial tension, ρ_{dp} and ρ_{cp} the dispersed and continuous phase densities, respectively, and η_{dp} and η_{cp} the dispersed and continuous phase viscosities. γ was measured for all systems by the rising drop method, with a tensiometer (Tracker, I.T. Concept, Teclis). η_{dp} was measured at 25.1°C, with a Ubbelohde viscosimeter (AVS310, Schött-Gerade).

TABLE I: Investigated system composition and physicochemical properties. Reproduced from A. Bertrandias, H. Duval, J. Casalinho and M. L. Giorgi, Phys. Fluids, 28, 102103 (2016), with the permission of AIP Publishing.

System and symbol	Dispersed phase	η_{dp} (mPa.s)	ρ_{dp} (kg.m^{-3})	Continuous phase	η_{cp} (mPa.s)	ρ_{cp} (kg.m^{-3})	γ (mN.m^{-1})
Reference (◊)	Dodecane	1.34	750	Distilled water	0.89	997	50.7 ± 3.5[a]
1 (◈)	Dodecane	1.34	750	Distilled water and SDS (0.1 wt%)	0.89	997 ± 1.4[a]	22.3 ± 0.5[a,b]
2 (⧫)	Dodecane	1.34	750	Distilled water and SDS (2 wt%)	0.89	1001 ± 1.2[a]	6.6 ± 0.2[a,b]
3 (◅)	Dodecane (75 wt%) and paraffin (25 wt%)	1.79 ± 0.23[a]	772 ± 1.2[a]	Distilled water	0.89	997	53.5 ± 2.4[a]
4 (▻)	Dodecane (50 wt%) and paraffin (50 wt%)	3.24 ± 0.42[a]	790 ± 1.1[a]	Distilled water	0.89	997	50.0 ± 1.2[a]

The tabulated values [a] are measured experimentally; [b] correspond to those at the intermediate plateau.

An original setup was designed (Fig. 1). It consists in a cell with a horizontal channel through which the continuous phase flows. A vertical nozzle of inner diameter $D_p = 0.32$ mm emerges into the channel. The continuous phase is pumped in a closed cycle by a gear pump (MDG M15T3B, Iwaki Co.), perpendicular to the nozzle axis (cross-flow). The flow rate is adjusted (OVAL MIII LSF41, OVAL Corporation) with a 0.1 L.h^{-1} precision. The dispersed phase is forced through the nozzle with a syringe pump (PHD ULTRA, Harvard Apparatus) at a volumetric flow rate q_{dp} (accuracy ≤ 0.25%), giving a mean dispersed phase velocity in the nozzle v_{dp}. A cold light (KL 2500 LCD, Schott) illuminates the setup. A high-speed camera (v310, Phantom) allowing up to 3250 fps at full resolution (1280 × 800 px²) is mounted with a macro lens (Macro MP-E 65mm f/2.8, Canon) of magnification × 5. Images are captured through the cell windows and are analysed with ImageJ to obtain data such as drop size D_d, with the scale (238 px/mm) set by the nozzle outer diameter (433 ± 2 µm). Average relative standard deviations in drop diameters are of 3.4%, 8.7% and 7.7% in dripping, jet widening and narrowing, respectively.

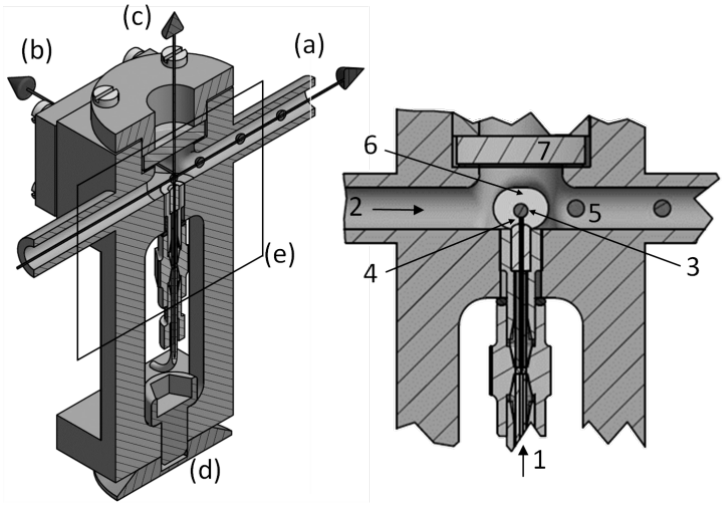

FIG. 1: Cell cross-section by CAD (to scale). Cell (left): (a) continuous phase flow axis; (b) optical axis; (c) dispersed phase flow axis; (d) cell binding point; (e) frame for zoom. Zoom in the cell (right): 1, dispersed phase inlet (microfluidic

system); 2, continuous phase flow; 3, growing drop; 4, nozzle; 5, formed drop carried away; 6, optical glass window; 7: window for user.

In order to obtain the so-called unperturbed continuous phase velocity at the location of the bound drop center of mass (denoted v_{cp}), the continuous phase flow is analyzed by particle image velocimetry (PIV), without dispersed phase injection (see supplementary material A, Fig. A1). Analysis is performed for the range of continuous phase volumetric flow rates q_{cp} tested in this work. The average continuous phase velocity is essentially uniform above the nozzle except in a thin adjacent layer (see supplementary material A, Fig. A2). We theoretically estimate the boundary-layer thickness at a distance $D_p/2$ from the leading edge of the nozzle[25] for all q_{cp} and find a thickness of 0.06 mm for the highest q_{cp} to 0.2 mm for the lowest q_{cp}: the boundary-layer thickness is always small compared to the minimum drop diameter formed at the given q_{cp} (0.302 mm and 1.019 mm, resp.). The drop is thus mainly located above the shear layer that develops above the nozzle. This differs from Meyer and Crocker's[21] or Pathak's[22] work, where the drop is entirely located in the shear flow set up by the continuous phase flowing parallel to the plane wall. In the following, the continuous phase velocity v_{cp} seen by a growing drop corresponds to the velocity measured in the uniform flow above the shear layer.

Drop formation by dripping is studied as a function of the continuous phase velocity v_{cp} seen by the growing drop. The parameters tested are reported in Table II (dripping trials). We consider that the Reynolds number characteristic of the continuous phase flow in the channel inside the cell is close to the Reynolds number in the cylindrical tubes on the sides of the cell, in series with this channel (see Fig. 1). We find $\mathrm{Re} = 4\rho_{cp}q_{cp}/\pi D_t\eta_{cp}$ from 330 to 3300, with D_t the tube diameter. According to Morrison[25], the continuous phase flow entering the cell is laminar ($\mathrm{Re} < 2100$) or transitional ($2100 < \mathrm{Re} < 3300$). The inner Reynolds number $\mathrm{Re_{in}} = 4\rho_{dp}q_{dp}/\pi D_p\eta_{dp}$ ranges from 2 to 38, so the dispersed phase flow is laminar in the nozzle.

Then, the DJT is studied. The v_{cp} values tested are given in Table II (DJT trials) and the dispersed phase velocity v_{dp} is increased slowly until the DJT. The onset of jetting is defined as in the literature[21,22]: it occurs when $L_n/D_d > 1$, with L_n the thread length prior to drop break off (from the nozzle surface to the drop base) and D_d the detached drop diameter. We obtain jetting velocities with a precision of 2.9 to 7.7% in jet widening and 2.6 to 11.1% in jet narrowing (due to the chosen increment in dispersed phase flux). We note that these velocities correspond to a transition from dripping to jetting. For the transition from jetting to dripping, the value may vary due to hysteresis phenomena.[11] $\mathrm{Re_{in}}$ ranges from 7 to 130, so the dispersed phase flow is laminar in the nozzle. In the tubes on the sides of the cell, Re ranges from 330 to 6600, so for the highest q_{cp}, *i.e.* v_{cp}, the continuous phase flow is turbulent in the channel.[25]

TABLE II: Operating conditions investigated.

System	Dripping trials		DJT trials
	v_{cp} (m.s^{-1})	v_{dp} (m.s^{-1})	v_{cp} (m.s^{-1})
Reference	0.18 - 0.55	0.016, 0.031, 0.063, 0.14, 0.21	0.17 - 1.03
1	0.11 - 0.50	0.031	0.17 - 0.59
2	0.10 - 0.40	0.031	0.17 - 0.40
3	0.11 - 0.55	0.031	0.23 - 1.03
4	0.10 - 0.60	0.031	0.23 - 0.94

After a series of trials (either PIV or dripping and DJT trials), the cell is filled with 3 vol% Mucasol (Merz) for 24h and is rinsed with distilled water. The nozzle surface is then hydrophilic: the organic dispersed phase does not wet the nozzle surface, so its outer diameter does not impact drop generation.

III. DROP GENERATION BY DRIPPING WITH CROSS-FLOW

Drop diameters D_d were measured as a function of the continuous phase velocity v_{cp} (Fig. 2), at constant v_{dp}= 0.031 m.s^{-1}. As v_{cp} increases, D_d decreases due to the increasing shear exerted by

the continuous phase flow. Drop diameters scale as $v_{cp}^{-0.62}$ to $v_{cp}^{-0.80}$, depending on the system. A lower interfacial tension γ leads to smaller drops (systems 1 and 2, Fig. 2). The capillary force decreases with γ, so a drop detaches earlier, also found by Xu *et al.*[26] No significant impact on D_d is seen with the dispersed phase viscosity η_{dp} (possibly a slight decrease in D_d with increasing η_{dp}) (Fig. 2). In membrane emulsification, Timgren *et al.*[27] numerically found a decrease in drop size with a thousand-fold increase in η_{dp}, expected as the drag coefficient then notably increases.[28] In our case, the difference may not be large enough to significantly impact drop size.

The influence of v_{dp} was also tested on the reference system (not shown). We find that v_{dp} does not impact drop diameter, as found for a stationary outer phase[29] or in cross-flow[26]. For these trials, drops form in dripping mode. $\mathrm{Ca_{out}} = \eta_{cp} v_{cp}/\gamma$ ranges from 3.1×10^{-3} to 9.7×10^{-3}, $\mathrm{We_{in}} = \rho_{dp} D_p v_{dp}^2/\gamma$ from 1.1×10^{-3} to 2.0×10^{-1} and $\mathrm{Oh}_{dp} = \eta_{dp}/\sqrt{\rho_{dp} D_p \gamma} = 1.2\times10^{-2}$. This is in fact in the dripping region of the state diagram reported in the literature.[21,22]

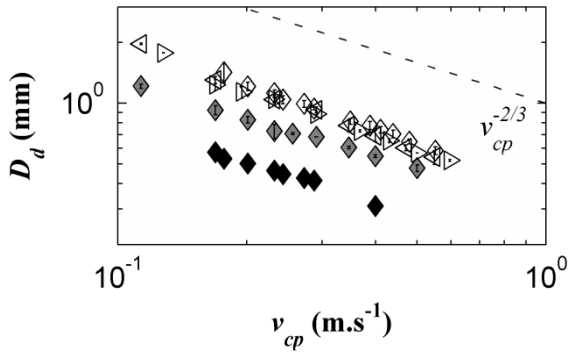

FIG. 2: Drop diameter D_d function of the continuous phase velocity v_{cp}, $v_{dp} = 0.031$ m.s^{-1}. See Table I for symbols.

In order to account for the drop diameter scaling observed in dripping mode, we consider that drag and the retaining capillary force are the main forces involved. Buoyancy is neglected since the buoyancy to drag force ratio is on average less than 5%. As Peng and Williams[2], we assume that the drop subjected to the forces discussed above stays spherical and rotates about the nozzle edge until detachment. The fraction of the drop that could remain attached to the nozzle tip after break off is neglected. The torque balance (TB) about the nozzle edge reads:

$$\frac{\pi D_d^2}{4} C_D \frac{\rho_{cp}}{2} v_{cp}^2 \frac{D_d}{2} = \pi D_p \gamma \frac{D_p}{2} \tag{1}$$

with C_D the drag coefficient. In Eq. (1), we neglect the velocity of the drop center of mass v_d. Indeed, if we assume that in dripping mode, the main contribution to the drop center of mass motion is due to drop growth, a rough estimate of v_d is given by $v_d(t) \approx 0.5(\mathrm{d}D_d/\mathrm{d}t)$, where D_d increases in time according to $D_d(t) = (6qt/\pi)^{1/3}$. For all systems and phase velocities tested, we find $v_d \ll v_{cp}$ (38 to 589 times). We further rearrange Eq. (1) as:

$$\frac{D_d}{D_p} = k \left(\frac{\mathrm{Oh}_{cp}}{\mathrm{Ca_{out}}} \right)^{2/3} \tag{2}$$

with $k = [8/C_D]^{1/3}$ and $\mathrm{Oh}_{cp} = \eta_{cp}/\sqrt{\rho_{cp} D_p \gamma}$ the outer Ohnesorge number. We note that Eq. (2) may also be written as $D_d/D_p = k\,\mathrm{We_{out}}^{-1/3}$, with $\mathrm{We_{out}}$ the outer Weber number, built with the continuous phase velocity. If we assume that C_D is approximately constant (corresponding to the Newton regime), from Eq. (2), we find that the drop diameter scales as $v_{cp}^{-2/3}$. This is in good agreement with our experimental data ($v_{cp}^{-0.62}$ to $v_{cp}^{-0.80}$). However, this scaling differs from the one found by Meyer and Crocker[21], *i.e.* $D_d/D_p \sim \mathrm{Ca_{out}}^{-1/2}$. In their trials, drops are entirely located in the shear layer that develops along the plane wall and their diameters seem better described by a force balance.

For a solid sphere in an infinite fluid, the Newton regime holds for particle Reynolds numbers $\mathrm{Re_p} = \rho_{cp} v_{cp} D_d/\eta_{cp}$ from 10^3 to 10^5.[25] In this range, $C_D \approx 0.4$. In our case, $\mathrm{Re_p} = 92$ to 360, so C_D

may vary. We estimate C_D from Eq. (1) and find that C_D decreases with increasing $\mathrm{Re_p}$ (data points, Fig. 3). Our C_D values are higher than reported for a viscous sphere in an infinite fluid by Feng and Michaelides[30] (dashed line, Fig. 3). Indeed, in our trials, the drop is not isolated but bound to a nozzle. We propose to model the variations of C_D as a function of $\mathrm{Re_p}$ by the law of Eq. (3), in the form obtained by Abraham[31] for a solid sphere:

$$C_D = C_0\left(1+\frac{\delta_0}{\mathrm{Re_p}^{1/2}}\right)^2 \tag{3}$$

We perform a weighted least squares minimization to identify the free coefficients of Eq. (3) from the data of the reference system, systems 1 and 2. These systems are characterized by a viscosity ratio $\zeta = 1.5$, with $\mathrm{Re_p} = 92$ to 360. We find $C_0 = 0.14$ and $\delta_0 = 17.7$. The data are well described by the adjusted law (solid line, Fig. 3). In the Stokes limit ($\mathrm{Re_p} \ll 1$), Eq. (3) reads $C_D \approx C_0\delta_0^2/\mathrm{Re_p} \approx 45/\mathrm{Re_p}$ close to the drag coefficient of a solid sphere at a wall in creeping flow, *i.e.* $C_D \approx 1.7\times(24/\mathrm{Re_p}) \approx 41/\mathrm{Re_p}$.[32] We only retain that the order is satisfactory as our drop deviates from a solid sphere and the coefficients were adjusted far from the Stokes regime.

For system 3 ($\zeta = 2.0$) and 4 ($\zeta = 3.6$), we cannot carry out the above method since our trials do not cover a wide range of $\mathrm{Re_p}$ for these viscosity ratios. We assume that C_D are not significantly different than from Eq. (3) fitted on systems with $\zeta = 1.5$, consistently with the analysis of Fig. 2. In Section IV, Eq. (3) will be used to estimate the drag force experienced by a drop near the DJT.

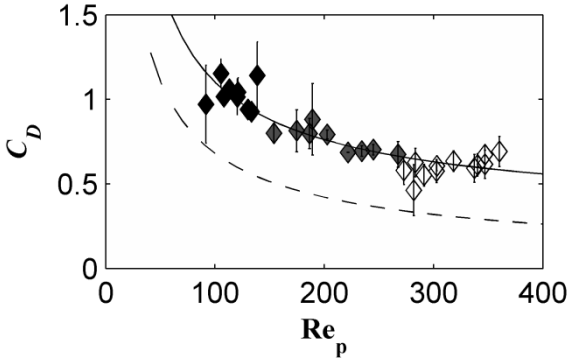

FIG. 3: Drag coefficient C_D function of the particle Reynolds number $\mathrm{Re_p}$. Experimental results from Eq. (1), see Table I for symbols. Feng and Michaelides predictions for $\zeta = 1.5$ (dashed line); our fit from Eq. (3) with $C_0 = 0.14$ and $\delta_0 = 17.7$ (solid line).

IV. DRIPPING TO JETTING TRANSITION (DJT)

A. Experimental results

For a set system and continuous phase velocity v_{cp}, the DJT is reached for a critical dispersed phase velocity (corresponding to the jetting velocity for the given v_{cp}). We remind that the onset of jetting is defined when the length of the liquid thread connecting the drop to the nozzle reaches the drop diameter (see Section II). Typical snapshots of dripping and jetting are reported in Fig. 4. We note that in Fig. 4(a) and (b), the first image on the left represents "strict" dripping (as studied in Section III), with a drop rotating about the nozzle edge.

As in coflowing liquids,[3,4,14] when the DJT is reached, two jetting regimes may be observed. When $v_{cp} \lesssim v_{dp}$, the liquid thread is on average thicker than the nozzle inner diameter (Fig. 4(a), last image): this is the widening regime. On the contrary, when $v_{cp} \gtrsim v_{dp}$, the liquid thread gets thinner from the nozzle to the drop (Fig. 4(b), last image): this is the narrowing regime. Curiously, Meyer and Crocker[21] did not distinguish these regimes in their paper.

In jet widening, we also see that the thread undergoes surface oscillations (see supplementary material B, Fig. B1). These oscillations are essentially stationary in space. According to Utada *et al.*[20] who studied jet widening in coflowing liquids, this behavior is characteristic of an absolute instability. To quantify this, as Utada *et al.*[20], we examine the variations of the neck diameter (between the thread and growing drop) as a function of time (see supplementary material B, Fig. B2). The neck diameter oscillates about its mean with an increasing amplitude until pinch off and

subsequent drop detachment. The oscillation frequency is around 350 Hz for the reference system, consistent with the inertial-capillary time scale of this system.

As for coflowing or cross-flowing liquids[3,21,22], we represent the DJT in the $\mathrm{Ca_{out}}-\mathrm{We_{in}}$ space. We remind that $\mathrm{We_{in}}$ is the inner Weber number ($\mathrm{We_{in}} = \rho_{dp} D_p v_{dp}^2/\gamma$) and $\mathrm{Ca_{out}}$ the outer capillary number ($\mathrm{Ca_{out}} = \eta_{cp} v_{cp}/\gamma$). Figure 5(a) presents the variations of $\mathrm{We_{in}}$ built with the jetting velocity as a function of $\mathrm{Ca_{out}}$, for the five systems of Table II. The curves exhibit a plateau for lower $\mathrm{Ca_{out}}$ values and a sudden decrease for higher $\mathrm{Ca_{out}}$. They are similar in shape to the curves established by Meyer and Crocker[21] and Pathak.[22] We associate the plateau with jet widening and the sudden decrease with jet narrowing. For all systems, at the plateau, $\mathrm{We_{in}}$ is in the order of 1, in the order of magnitude reported for jet widening in coflow.[3] Our plateau values are also similar to those of Meyer and Crocker[21] and Pathak.[22] The transition between widening and narrowing occurs at a critical value of $\mathrm{Ca_{out}}$, such that $v_{cp} \approx v_{dp}$. This value is denoted Ca^* for the reference system in Fig. 5(a).

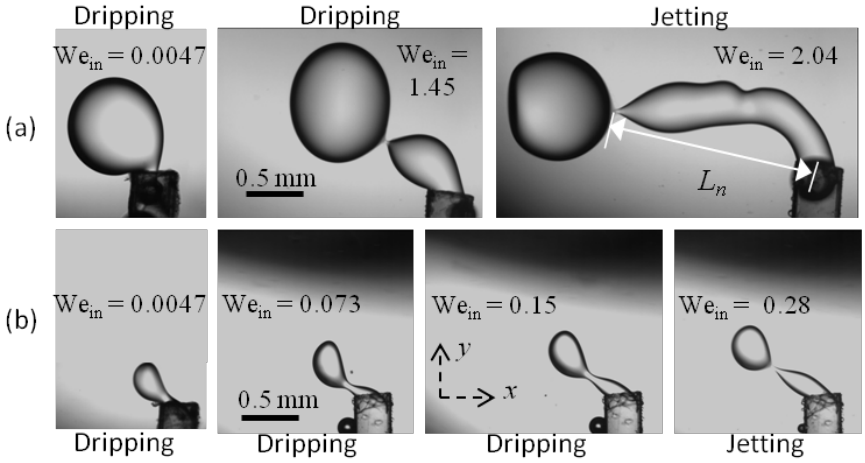

FIG. 4: Reference system snapshots ($\mathrm{Oh}_{cp} = 7.0\times10^{-3}$): (a) jet widening, $\mathrm{Ca_{out}} = 5.1\times10^{-3}$; (b) jet narrowing, $\mathrm{Ca_{out}} = 1.3\times10^{-2}$. Continuous phase flow from right to left.

The same trends, *i.e.* a plateau followed by a marked decrease, are obtained for the drop diameters formed at the DJT as a function of $\mathrm{Ca_{out}}$ (Fig. 5(b)). The variations in drop diameters at the DJT as a function of $\mathrm{Ca_{out}}$ were not reported before.[21,22] In jet widening, we expect that the drop diameter is controlled by a balance between the jet momentum and the retaining capillary force. In jet narrowing, the drop diameter should be controlled by a balance between the drag force experienced by the drop and the capillary force. As the continuous phase velocity increases, the thread gets thinner leading to a lower retaining capillary force, thus smaller drops.

As the interfacial tension γ decreases between the reference system, system 1 and 2, the plateau value for $\mathrm{We_{in}}$ decreases and the transition from jet widening to narrowing is shifted towards higher $\mathrm{Ca_{out}}$. This result, to which we shall return, was not reported before. The influence of γ on the DJT was not examined in detail in cross-flow.[21,22]

In our trials, the dispersed phase viscosity η_{dp} does not affect the jetting velocity since the data for the reference system, system 3 and 4 collapse onto a unique curve (Fig. 5(a)). This is in good agreement with Meyer and Crocker's results.[21] They found that the jetting velocity does not vary significantly with the inner Ohnesorge number $\mathrm{Oh}_{dp} = \eta_{dp}/\sqrt{\rho_{dp} D_p \gamma}$ while Oh_{dp} is below 3×10^{-2}. Indeed, while $\mathrm{Oh}_{dp} \ll 1$, the pinch-off time scale is in the order of the inertial-capillary time scale, thus it does not depend on η_{dp}. This corresponds to our experimental range: Oh_{dp} increases from 1.2×10^{-2} to 2.9×10^{-2} as η_{dp} increases from 1.34 to 3.24 mPa.s. Drop diameters are also unaffected by η_{dp} (Fig. 5(b)).

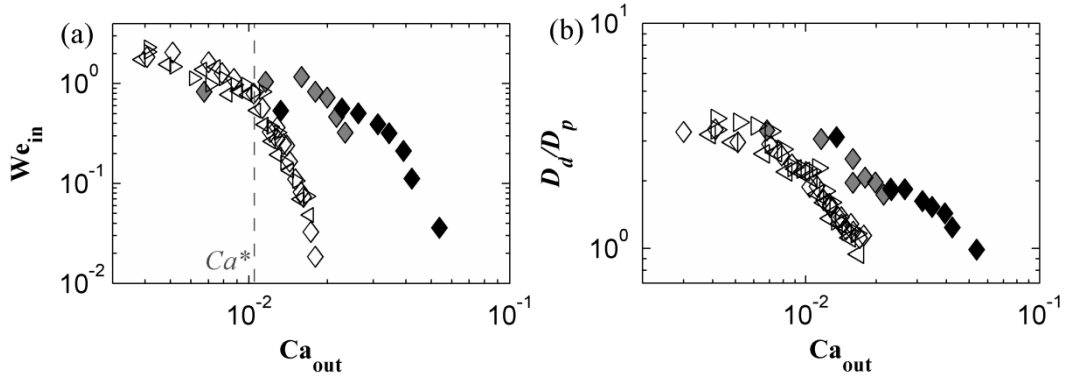

FIG. 5: Characteristic values at the DJT, see Table I for symbols: (a) $\mathrm{We_{in}}$ function of $\mathrm{Ca_{out}}$. Widening to narrowing limit Ca^* for the reference system (dashed line); (b) Drop to pore diameter ratio D_d/D_p function of $\mathrm{Ca_{out}}$.

According to Utada *et al.*[3] and Meyer and Crocker[21], our DJT curves should overlap in the $\mathrm{Ca_{out}}-\mathrm{We_{in}}$ space since $\mathrm{Oh}_{dp} \ll 1$. However, as stated before, our DJT curves are shifted towards higher $\mathrm{Ca_{out}}$ as the interfacial tension decreases. We attribute this to the hydrodynamic regime of the drag force experienced by a growing drop. Indeed, the particle Reynolds number $\mathrm{Re_p}$ ranges from 114 to 424 in our DJT trials. These values are much higher than those reported by Utada *et al.*[3] and Meyer and Crocker.[21] Thus, the drag force in our trials rather corresponds to the Newtonian regime than to the Stokes regime. Since the ratio of the drag to capillary force is in the order of $(\mathrm{Ca_{out}}/\mathrm{Oh}_{cp})^2 = \mathrm{We_{out}}$ under Newton regime assumption (as opposed to $\mathrm{Ca_{out}}$ under Stokes approximation), we plot $\mathrm{We_{in}}$ as a function of $\mathrm{Ca_{out}}/\mathrm{Oh}_{cp}$ (see supplementary material C). We remind that Oh_{cp} is the outer Ohnesorge number ($\mathrm{Oh}_{cp} = \eta_{cp}/\sqrt{\rho_{cp} D_p \gamma}$). We find that reference system and system 1 and 2 data then actually collapse in the narrowing regime.

B. Model

The DJT criteria proposed by Pathak[22] and Meyer and Crocker[21] are not adapted to our case. Indeed, in our trials, the growing drops are mainly located above the shear layer adjacent to the nozzle tip (see Section II) and the particle Reynolds number is far from the Stokes regime (see Section IV.A). Figure D1 (supplementary material D) shows the discrepancy between our DJT data for the reference system and previous authors' DJT criteria.[21,22] We remind that these criteria are semi-empirical since these authors simply replaced Bo and $\mathrm{Bo_o}$, the Bond numbers built with the nozzle inner and outer diameters, by $\mathrm{Ca_{out}}$ in Clanet and Lasheras' criterion[11] and adjusted the coefficients to fit their data. In this section, we propose a comprehensive model to account for the jetting velocity and drop diameters at the DJT.

Firstly, the footage shows that thread dynamics occur essentially along the x-axis (Fig. 4): the drop forms at the end of a thread that tends to align with the continuous phase flow. Thus, we approximate our configuration by a coflow configuration (Fig. 6). A force balance is now more relevant than a torque balance since the drop can no longer be considered as a sphere rotating about the nozzle edge.

We revisit Clanet and Lasheras' approach[11] developed for a liquid injected downwards into a stagnant gas under gravity and amend the drop equation of motion to consider coflowing liquids. We thus add a drag force induced by the continuous flowing phase since η_{cp} is orders of magnitude higher than the dynamic viscosity of air and we account for the added mass effect since $\rho_{cp} \sim \rho_{dp}$. We neglect buoyancy since for the largest drops (obtained in the widening regime), the buoyancy to capillary force ratio is lower than 3%.

In Clanet and Lasheras' scenario[11], drops are generated as follows: a first drop detaches (at $x = 0$ in Fig. 6), leaving a thread behind that recedes at a velocity $\mathrm{d}x/\mathrm{d}t$, due to surface tension effects. During recession, a mass (drop) M forms (sphere in Fig. 6). It recedes until it reaches a distance x_{max} (closer to the nozzle, Fig. 6). The mass then progresses the other way, once momentum and drag overcome surface tension effects. It is assumed that pinch off begins at x_{max}. From that point, the drop no longer grows. The drop travels a distance l_d until detachment. If $x_{max} > l_d$, dripping occurs. Oppositely, if $x_{max} < l_d$, the detachment point advances each time, leading to jetting.

The mass $M(t)$ of the drop is given by

$$M(t) = \frac{\pi}{4} D_p^2 \, \rho_{dp} v_{dp} t + \rho_{dp} \int_0^{x(t)} S_{th}(x') \, dx' \tag{4}$$

We remind that v_{cp} and v_{dp} are velocity moduli. $S_{th}(x)$ is the thread cross-section at the location x. $S_{th}(x)$ is related to $v_{th}(x)$, the mean fluid velocity modulus in the thread at the location x, by $q_{dp} = S_{th}(x) v_{th}(x)$. The variations of the mean dispersed phase velocity v_{th} along the thread depend on the continuous phase shear stress.

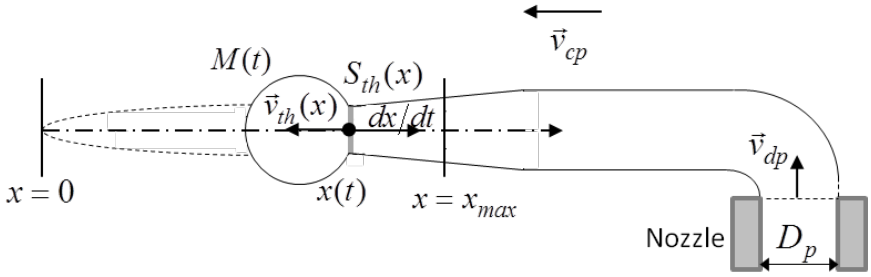

FIG. 6: Model configuration with the different variables involved.

The drop equation of motion during recession reads:

$$\frac{\mathrm{d}}{\mathrm{d}t}\left[(M(t) + M_a(t))\frac{\mathrm{d}x}{\mathrm{d}t}\right] = \pi D_{th}(x)\gamma - \rho_{dp} q_{dp}\left(\frac{\mathrm{d}x}{\mathrm{d}t} + v_{th}(x)\right) - \frac{\pi}{4} D_m^2(t) C_D \frac{\rho_{cp}}{2}\left(v_{cp} + \frac{\mathrm{d}x}{\mathrm{d}t}\right)^2 \tag{5}$$

The left-hand side of Eq. (5) corresponds to the drop effective inertia and includes $M_a(t)$ the added mass due to the surrounding continuous phase. We suppose that the added mass is equal to half of the displaced volume of continuous phase, as for a solid sphere in an infinite medium. It is thus given by $M_a(t) = 0.5 M(t) \rho_{cp}/\rho_{dp}$. The first term on the right-hand side of Eq. (5) is the retaining capillary force, with $D_{th}(x)$ the thread diameter at the location x. The second term is the jet momentum flux entering the drop. The last term is the drag force, in which the frontal area corresponds to that of a sphere with the given mass. The drop mass diameter is given by:

$$D_m(t) = \left[\frac{6}{\pi}\frac{M(t)}{\rho_{dp}}\right]^{1/3} \tag{6}$$

In the drag force, the drag coefficient $C_D(\mathrm{Re_p})$ is estimated from Eq. (3), with the coefficients adjusted before and $\mathrm{Re_p}$ is built with $D_m(t)$ (Eq. (6)) and the relative velocity $\left|v_{cp} + \mathrm{d}x/\mathrm{d}t\right|$. At the DJT, we find $\mathrm{Re_p} = 114$ to 424 (estimated with the experimental D_d and v_{cp}). This is in the same range as where the coefficients of Eq. (3) were adjusted. However, Eq. (3) was established for drops detaching in dripping mode: we here neglect the deviations in C_D that may arise at the DJT when the thread linking the drop to the nozzle is larger. We assume that C_D essentially depends on the drop mass diameter and the particle Reynolds number and little on the drop shape details.

x_{max} is determined from the numerical integration of system (4-6) (see Appendix). As stated above, the DJT occurs at $x_{max} = l_d$. l_d is the detachment distance by pinch off, such that:

$$\int_0^{l_d} \frac{\mathrm{d}x}{v_{th}(x)} = \tau_n \tag{7}$$

τ_n is the necking time or pinch-off time (in the order of the inertial-capillary time), given by:

$$\tau_n = k'\left[\frac{D_j^3(x_{max})\rho_{dp}}{8\gamma}\right]^{1/2} \tag{8}$$

We estimate $k' \approx 8.26 \pm 0.43$ by Clanet and Lasheras' method[11]: we measure the neck diameter variations in dripping mode as a function of time during pinch off, we fit the variations to an exponential form to find τ_n and we plot $1/\tau_n$ as a function of $\tau_c = \left[8\gamma/D_p^3\rho_{dp}\right]^{1/2}$. This was done for the reference system, systems 1 and 2 (see supplementary material E). These systems differ only by their interfacial tension and are characterized by a viscosity ratio $\zeta = 1.5$. We find τ_n 2.6 times

higher than Clanet and Lasheras[11] for a liquid in air, which depicts a lower instability growth rate. This is in agreement with results reported in the literature: Rayleigh[33] found a growth rate (made dimensionless by τ_c) of 0.34 for an inviscid liquid in air. On the other hand, Funada and Joseph[34] found a growth rate 1.3 to 4.8 times lower for water in benzene ($\zeta = 1.5$) in the range of our $\mathrm{Re_{in}}$, from a fully viscous analysis.

Returning to the model, the jetting velocity at a set v_{cp} is obtained as follows (see Appendix for details): v_{dp} is scanned and for each v_{dp}, the system (4-6) is integrated as a function of time, until $x = x_{max}$. If x_{max} coincides with l_d (Eq. (7)), the corresponding v_{dp} value is the jetting velocity at the given v_{cp}. The resulting drop diameter is deduced from Eq. (6): $D_d \approx D_m(t_{max})$, where t_{max} is the time taken for the mass to travel from 0 to x_{max}. This method may be repeated for each v_{cp} tested to reproduce our experimental results.

C. Comparison with experiments

To implement the above model, we must describe the mean dispersed phase velocity along the thread. Two limit cases will be considered: (1) the thread diameter and mean velocity are negligibly affected by the continuous phase flow in both jetting regimes and (2) the mean thread velocity quickly reaches the continuous phase velocity in the narrowing regime.

C.1. Uniform nozzle-sized thread

First, we consider the simplest scenario where the thread diameter is not affected by the continuous phase in either jetting regime. In this case, we assume $v_{th}(x) = v_{dp}$ and $D_{th}(x) = D_p$ from $x = 0$ to x_{max}. Then, the thread cross-section reads $S_{th}(x) = \pi D_p^2/4$. We call this the uniform nozzle-sized thread limit. We solve system (4-6) under this assumption by the method described in the Appendix. The results are reported in Fig. 7 (solid lines).

The variations of the critical inner Weber number $\mathrm{We_{in}}$ function of the outer capillary number $\mathrm{Ca_{out}}$ are satisfactorily reproduced (Fig. 7(a), solid lines). The same conclusion may be drawn for the variations of the dimensionless drop diameter as a function of $\mathrm{Ca_{out}}$ (Fig. 7(b), solid lines). Furthermore, the effect of the interfacial tension on the transition is well accounted for.

The model predicts a plateau in jet widening (for small $\mathrm{Ca_{out}}$), but in our experiments, the plateau is more pronounced and extends for higher $\mathrm{Ca_{out}}$. Furthermore, in jet widening, $\mathrm{We_{in}}$ and especially D_d are overpredicted. The difference in plateau values for $\mathrm{We_{in}}$ between the reference system and system 2 is also not reproduced (Fig. 7(a)). We checked that the differences in plateau values cannot be attributed to the relative effect of buoyancy. We attribute them to the thread surface oscillations (see supplementary material B), which affect the retaining capillary force and pinch-off time. These oscillations cannot be accounted for in the framework of the present model.

Lastly, we note that $\mathrm{We_{in}}$ and D_d are overestimated at high $\mathrm{Ca_{out}}$ for the reference system (and systems 3 and 4, not shown in Fig. 7). This may be explained by the narrowing of the thread which becomes significant at high v_{cp} but is neglected in the present case. In the next section (IV.C.2), we attempt to take this effect into account.

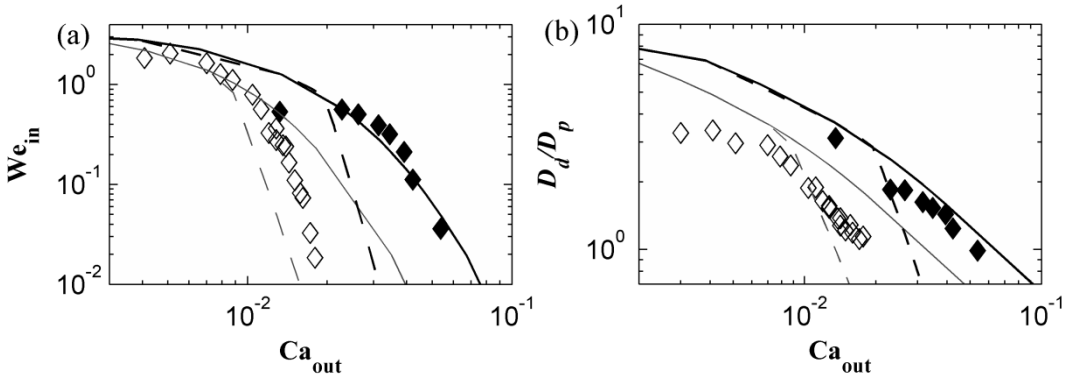

FIG. 7: Characteristic values at the DJT, see Table I for symbols. (a) $\mathrm{We_{in}}$ function of $\mathrm{Ca_{out}}$. (b) Drop to pore diameter ratio D_d/D_p function of $\mathrm{Ca_{out}}$. Simulation results for the reference system (grey); system 2 (black). Uniform nozzle-sized thread limit of Section IV.C.1 (solid line); maximal narrowing limit of Section IV.C.2 (dashed line).

C.2. Maximal narrowing

We measure the thread diameter for the reference system in the narrowing regime: it decreases by less than 10% for $v_{cp} \leq 0.73$ m.s^{-1} ($Ca_{out} = 1.3\times10^{-2}$) but decreases by more than 50% for the highest v_{cp}. In the latter case, narrowing effects can no longer be neglected and our hypothesis $D_{th}(x) = D_p$ of Section IV.C.1 is no longer valid.

We suppose that the momentum diffusion across the thread is rapid and fully efficient in the narrowing regime. In this case, we may consider that if $v_{cp} > v_{dp}$, the thread is characterized by $v_{th}(x) = v_{cp}$, $D_{th}(x) = D_p(v_{dp}/v_{cp})^{1/2}$ and $S_{th}(x) = \pi D_{th}^2(x)/4$ from $x = 0$ to x_{max}. This gives the maximal narrowing limit. According to Castro-Hernandez *et al.*[4], maximal narrowing is observed when $Re_{in} < 1$. In our trials, $Re_{in} = 7$ to 130, so their assumption is not strictly applicable. However, it will give us an overestimate of the narrowing effect on the DJT and drop diameter. If $v_{cp} < v_{dp}$ (jet widening), we still neglect the effect of the continuous phase on the thread size and assume that $D_{th}(x) = D_p$ and $v_{th}(x) = v_{dp}$, as in Section IV.C.1.

As before, we solve system (4-6) under these new assumptions (see Appendix) and we report the results in Fig. 7 (dashed lines). For the reference system (and systems 3 and 4, not shown), our data for We_{in} and D_d in jet narrowing lie in between the maximal narrowing limit (dashed lines, Fig. 7(a) and (b)) and the uniform nozzle-sized thread limit (solid lines, Fig. 7(a) and (b)).

We note that the data for system 2 are surprisingly well described by the uniform nozzle-sized thread limit. This is probably due to the compensation of different errors related to the uniform nozzle-sized approximation, the use of the drag coefficient estimated in the dripping regime and the assumption that forces act only along the x-axis.

V. CONCLUSIONS

While the dripping to jetting transition (DJT) is well documented for liquid-air[8,11] or liquid-liquid coflow[3,4,13,14], liquid-liquid cross-flow[21,22] has received little attention and no comprehensive model was proposed to describe the DJT in this configuration. Also, drop diameters specifically at the DJT were either not measured or not reported.[21,22]

In the present work, we studied liquid-liquid cross-flow for different phase velocities, interfacial tensions and dispersed phase viscosities. Contrary to previous work[21,22], the growing drops are mainly located above the shear layer that develops above the nozzle. Furthermore, since the inner Ohnesorge number (characteristic of the dispersed phase flow) is much lower than 1, drop pinch-off is controlled by the inertial-capillary time scale.

In strict dripping, we found that the drop diameter is well described by a simple torque balance about the nozzle edge, taking into account the drag force experienced by the drop and the retaining capillary force. This result was used to estimate the drag coefficient for an attached drop as a function of the particle Reynolds number.

The DJT occurs at a critical inner Weber number function of the outer capillary and Ohnesorge numbers. Two jetting regimes occur (widening and narrowing) depending on the phase velocity ratio. In jet widening (when the dispersed phase velocity is greater than the continuous phase one), the critical inner Weber number depends little on the outer capillary number whereas in the narrowing regime, it sharply decreases as the outer capillary number increases. Furthermore, when the outer Ohnesorge number increases, the transition between widening and narrowing is shifted to higher values of the outer capillary number. The hydrodynamic regime of the drag force experienced by a growing drop is actually inertial and not viscous.

We proposed to model the DJT in liquid-liquid cross-flow by revisiting an approach originally developed by Clanet and Lasheras for a liquid injected into a stagnant gas under gravity. The model describes the recession dynamics and the growth of the drop until pinch off. In the present case, the driving force for drop detachment is not buoyancy but the drag force exerted by the continuous phase flow. We distinguished two limit cases for the thread profile that exits the nozzle and enters the drop: a uniform nozzle-sized thread limit and a maximal narrowing limit. Jetting velocities and drop diameters measured at the DJT in jet narrowing are well accounted for and lie in between model predictions in the two limit cases. Furthermore, the effect of the outer Ohnesorge number on the DJT is well reproduced. In jet widening, the agreement is less satisfactory. Discrepancies are attributed to thread surface oscillations which appear in jet widening. However, we may conclude that the main

features of the DJT in cross-flow are captured which highlights the insight and the robustness of Clanet and Lasheras' original model.

SUPPLEMENTARY MATERIAL

See supplementary material for insight on: A, continuous phase flow analysis using Particle Image Velocimetry (PIV); B, oscillations in jet widening; C, collapsed data in jet narrowing; D, comparison with Pathak's and Meyer and Crocker's DJT criteria; E, estimation of the necking time.

ACKNOWLEDGEMENTS

We thank T. Martin and J. Trubuil for their contribution in designing the setup and for their work on the setup manufacturing.

APPENDIX: NUMERICAL METHOD TO OBTAIN THE JETTING VELOCITY

For a set v_{cp}, the jetting velocity is obtained by an iterative procedure. v_{dp} is varied with a 0.001 m.s^{-1} increment. For each v_{dp} value, the recession dynamics of a growing drop is computed by integrating system (4-6) using the fourth order Runge-Kutta method. The initial conditions are $D_d(0) = 0$ and $x(0) = 0$. According to Eq. (5), $\dot{x}(0)$ is then given by Eq. (A1) for the uniform nozzle-sized thread limit and by Eq. (A2) for the maximal narrowing limit.

$$\dot{x}(0) = -\frac{v_{dp}}{2}\left(1+\frac{\rho_{dp}}{\rho_e}\right) + \frac{1}{2}\left(v_{dp}^2\left(1-\frac{\rho_{dp}}{\rho_e}\right)^2 + \frac{16\gamma}{D_p\rho_e}\right)^{1/2} \qquad (A1)$$

$$\dot{x}(0) = -\frac{v_{cp}}{2}\left(1+\frac{\rho_{dp}}{\rho_e}\right) + \frac{1}{2}\left(v_{cp}^2\left(1-\frac{\rho_{dp}}{\rho_e}\right)^2 + \frac{16\gamma\left(v_{dp}/v_{cp}\right)^{1/2}}{D_p\rho_e}\right)^{1/2} \qquad (A2)$$

with $\rho_e = \rho_{dp} + \rho_{cp}/2$. Integration is performed until the drop stops and changes direction. That point is denoted x_{max}. The above iterative procedure is stopped as soon as $x_{max} = l_d$, the latter calculated from Eq. (7). At this point, the v_{dp} value corresponds to the jetting velocity.

[1] T. Nakashima, M. Shimizu and M. Kukizaki, "Membrane Emulsification by Microporous Glass," Key Eng. Mat. **61-62**, 513 (1992).

[2] S. J. Peng and R. A. Williams, "Controlled production of emulsions using a crossflow membrane: Part I: Droplet formation from a single pore," Chem. Eng. Res. Des. **76** (8), 894 (1998).

[3] A. Utada, A. Fernandez-Nieves, H. Stone and D. Weitz, "Dripping to Jetting Transitions in Coflowing Liquid Streams," Phys. Rev. Lett. **99** (9), 094502 (2007).

[4] E. Castro-Hernández, V. Gundabala, A. Fernández-Nieves and J. M. Gordillo, "Scaling the drop size in coflow experiments," New J. Phys. **11** (7), 075021 (2009).

[5] A. M. Gañán-Calvo, "Jetting–dripping transition of a liquid jet in a lower viscosity co-flowing immiscible liquid: the minimum flow rate in flow focusing," J. Fluid Mech. **553** (1), 75 (2006).

[6] S. L. Anna, N. Bontoux and H. A. Stone, "Formation of dispersions using "flow focusing" in microchannels," Appl. Phys. Lett. **82** (3), 364 (2003).

[7] A. S. Utada, "Monodisperse Double Emulsions Generated from a Microcapillary Device," Science **308** (5721), 537 (2005).

[8] S. W. J. Smith and H. Moss, "Experiments with Mercury Jets," Proc. R. Soc. Math. Phys. Eng. Sci. **93** (652), 373 (1917).

[9] G. F. Scheele and B. J. Meister, "Drop formation at low velocities in liquid-liquid systems: Part II. Prediction of jetting velocity," AIChE J. **14** (1), 15 (1968).

[10] J. R. Richards, A. N. Beris and A. M. Lenhoff , "Drop formation in liquid–liquid systems before and after jetting," Phys. Fluids **7** (11), 2617 (1995)

[11] C. Clanet and J.C. Lasheras, "Transition from dripping to jetting," J. Fluid Mech. **383**, 307 (1999).

[12] G. I. Taylor, "The dynamics of thin sheets of fluids. III. Disintegration of fluid sheets," Proc. R. Soc. Lond. A **253**, 313 (1959).

[13] C. Cramer, P. Fischer and E. J. Windhab, "Drop formation in a co-flowing ambient fluid," Chem. Eng. Sci. **59** (15), 3045 (2004).

[14] Y. Chen, L. Wu and C. Zhang, "Emulsion droplet formation in coflowing liquid streams," Phys. Rev. E **87** (1), 013002 (2013).
[15] S. J. Leib and M. E. Goldstein, "Convective and absolute instability of a viscous liquid jet," Phys. Fluids **29** (4), 952 (1986).
[16] P. Huerre and P. A. Monkewitz, "Local and Global Instabilities in Spatially Developing Flows," Annu. Rev. Fluid Mech. **22** (1), 473 (1990).
[17] P. Guillot, A. Colin, A. S. Utada and A. Ajdari, "Stability of a Jet in Confined Pressure-Driven Biphasic Flows at Low Reynolds Numbers," Phys. Rev. Lett. **99** (10), 104502 (2007).
[18] P. Guillot, A. Colin and A. Ajdari, "Stability of a jet in confined pressure-driven biphasic flows at low Reynolds number in various geometries," Phys. Rev. E **78** (1), 016307 (2008).
[19] M. A. Herrada, A. M. Gañán-Calvo and P. Guillot, "Spatiotemporal instability of a confined capillary jet," Phys. Rev. E **78** (4), 046312 (2008).
[20] A. S. Utada, A. Fernandez-Nieves, J. M. Gordillo and D. A. Weitz, "Absolute Instability of a Liquid Jet in a Coflowing Stream," Phys. Rev. Lett. **100** (1), 014502 (2008).
[21] R. F. Meyer and J. C. Crocker, "Universal Dripping and Jetting in a Transverse Shear Flow," Phys. Rev.Lett. **102**, 194501 (2009).
[22] M. Pathak, "Numerical simulation of membrane emulsification: Effect of flow properties in the transition from dripping to jetting," J. Membr. Sci. **382** (1–2), 166 (2011).
[23] S. R. Deshiikan, D. Bush, E. Eschenazi and K. D. Papadopoulos, "SDS, Brij58 and CTAB at the dodecane-water interface," Colloids and Surfaces A: Physicochem. Eng. Aspects **136**, 133 (1998).
[24] A. Bertrandias, H. Duval, J. Casalinho and M. L. Giorgi, "Drop generation from a vibrating nozzle in an immiscible liquid-liquid system," Phys. Fluids **28**, 102103 (2016).
[25] F. A. Morrison, *An introduction to fluid mechanics* (Cambridge University Press, 2013), pp. 622–694.
[26] J. Xu, G. Luo, G. Chen and J. Wang, "Experimental and theoretical approaches on droplet formation from a micrometer screen hole," J. Membr. Sci. **266** (1–2), 121 (2005).
[27] A. Timgren, G. Trägårdh and C. Trägårdh, "Effects of cross-flow velocity, capillary pressure and oil viscosity on oil-in-water drop formation from a capillary," Chem. Eng. Sci. **64** (6), 1111 (2009).
[28] R. Clift, J. Grace and M. E. Weber, *Bubbles, Drops and Particles* (Dover Publications, Inc., 2005) pp.125–135.
[29] A. Bertrandias, H. Duval, J. Casalinho and M. L. Giorgi, "Good vibrations —Transition in drop generation from an immersed capillary tube," EPL **111** (4), 44004 (2015).
[30] Z.-G. Feng and E. E. Michaelides, "Drag Coefficients of Viscous Spheres at Intermediate and High Reynolds Numbers," J. Fluids Eng. **123** (4), 841 (2001).
[31] F. F. Abraham, "Functional Dependence of Drag Coefficient of a Sphere on Reynolds Number," Phys. Fluids **13** (8), 2194 (1970).
[32] M. E. O'Neill, "A sphere in contact with a plane wall in a slow linear shear flow," Chem. Eng. Sci. **23** (11), 1293 (1968).
[33] Rayleigh, "On the instability of jets," Proceeding Lond. Math. Soc. **10**, 4 (1878).
[34] T. Funada and D. D. Joseph, "Viscous potential flow analysis of capillary instability," Int. J. Multiph. Flow **28** (9), 1459 (2002).